IEEE Transactions on Quantum Engineering

Received September 29, 2020; revised November 18, 2020; accepted December 8, 2020; date of publication December 18, 2020; date of current version January 14, 2021.

Digital Object Identifier 10.1109/TQE.2020.3045682

Josephson Microwave Sources Applied to Quantum Information Systems

ADAM J. SIROIS, MANUEL CASTELLANOS-BELTRAN, ANNA E. FOX (Senior Member, IEEE), SAMUEL P. BENZ (Fellow, IEEE), AND PETER F. HOPKINS (Senior Member, IEEE)

National Institute of Standards and Technology, Boulder, CO 80305 USA

This work was supported by the U.S. Department of Commerce's Quantum Initiative. Corresponding author: Adam J. Sirois (e-mail: sirois@nist.gov)

ABSTRACT Quantum computers with thousands or millions of qubits will require a scalable solution for qubit control and readout electronics. Colocating these electronics at millikelvin temperatures has been proposed and demonstrated, but there exist significant challenges with power dissipation, reproducibility, fidelity, and scalability. In this article, we experimentally demonstrate the use of a Josephson arbitrary waveform synthesizer (JAWS) to generate control signals at 4 K and perform spectroscopy of two components of a typical superconducting quantum information system: a linear resonator and a (nonlinear) transmon qubit. By locating the JAWS chip at 4 K and a qubit at 0.1 K, the direct path for quasi-particle poisoning from the JAWS chip to the qubit is broken. We demonstrate the stable, self-calibrated, and reproducible output signal of the JAWS when operated in its quantum locking range, a feature that allows these synthesizers to be replicated and scaled in the cryostat, all with identical on-chip, quantized, outputs. This is a proof-of-concept demonstration to generate signals at 4 K using driven superconducting electronics to control qubits at lower temperatures.

INDEX TERMS Arbitrary waveform, Josephson junction (JJ), quantum computing, spectroscopy, superconductor, transmon.

I. INTRODUCTION

Superconducting circuit quantum electrodynamics experiments form the basis for many quantum computing technologies [1]–[3]. Superconducting qubit systems are controlled using a mix of continuous-wave (CW) ac, pulse-shaped ac, and dc signals. These signals are generated at room temperature and are then routed into a dilution refrigerator where they are attenuated and thermalized to appropriate levels for the qubit(s). Experiments involve manipulating the state of a qubit with microwave-frequency waveforms and monitoring the phase or amplitude of a linear resonator to which the qubit is coupled. Rather than using only room temperature electronics, here we demonstrate the use of a superconducting Josephson arbitrary waveform synthesizer (JAWS) circuit to directly generate reproducible, quantum-based microwave signals at 4 K. Voltage sources based on Josephson junctions (JJs) provide reproducible and metrologically accurate reference signals when operated in their *quantum locking range* [4]. This range is roughly defined as the range the JAWS's output voltage is based on fundamental physics and is immune to changes in input and environmental parameters.

JJ-based digital logic elements—generally referred to here as single flux quantum (SFQ) electronics—have been proposed and initial demonstrations have shown them to be a potential solution to scaling quantum computing technologies to larger numbers of qubits [5]–[7]. These logic elements, when operated at ∼10 mK in close proximity to qubits, create fast pulses with quantized voltage-time area that can be used for high-fidelity qubit state preparation. One drawback to colocating the qubit and SFQ circuits is unwanted quasi-particles that are generated by the SFQ circuits because the generation of an SFQ pulse requires that the JJ briefly switch to the normal (resistive) state. These quasi-particles, in turn, reduce the coherence of the qubit(s) [8]. Physical separation of the SFQ electronics chip from the qubit chip is desirable for mitigation of this quasi-particle-induced decoherence. One configuration is to create a multi-chip module with the qubit chip and SFQ chip bump-bonded together using superconducting interconnects, thus avoiding substrate-to-substrate transmission of most quasi-particles via phonons [9]. Another option, explored here, is to locate the SFQ electronics at 4 K. This requires the generation of

larger amplitude signals at 4 K and then attenuation of those signals (for thermalization of noise and reduction of signal amplitude) as they are routed to the qubit(s) at ∼10 mK. Because the SFQ circuits are located far from the qubits, excess quasi-particles from the SFQ generation will not reach the qubit circuit. This approach also does not require multichip processing steps.

Another advantage of moving qubit control signal generation to 4 K may be in terms of performing low-latency feedback for future, large-scale, quantum computing systems [10]. Proposals for these types of systems indicate that feedback and digital signal processing circuitry (often described as a *quantum-classical interface*) cannot be located at the base temperature stage of the dilution refrigerator due to limited cooling power available [5]. Thus, in this article, we demonstrate a method for generating two potentially useful feedback signals, CW and SFQ-pulse voltage signals, at 4 K, where there is ample cooling power in modern dilution refrigerators (typically >1 W).

More practically, locating SFQ circuits at 4 K can be useful if the SFQ-generating circuit traps stray vortices near a JJ or inductor. Experimentally, the solution to *de-flux* a circuit is to warm it above the superconducting transition temperature of the metal, then recool it in the absence of a magnetic field. To heat a niobium circuit above the niobium critical temperature of ∼9 K from the 4 K stage of a dilution refrigerator is commonly done, doing so with a circuit anchored to the millikelvin stage of a dilution refrigerator would require heating the whole stage above the transition temperature of the qubits (commonly aluminum, $T_c = 1.2$ K) and the boiling point of the circulating helium mixture. In this case, recovery time to achieve base temperature and possibly recalibrate the qubit would be long. As discussed below, and shown in Fig. 1, our JAWS circuit does not include flux-quantizing inductors, such as SFQ-based logic elements do and, thus, are more tolerant to stray trapped flux as well [11]. This will become an important experimental concern when scaling to larger numbers of SFQ-based *or* JAWS-based qubit control.

II. JAWS DECRIPTION

The JAWS circuit used in this article is a thin-film niobium coplanar waveguide (CPW) transmission line with characteristic impedance of 50 Ω that has a series array of 102 uniform JJs shunting two 50 − Ω normal-metal resistors to ground. The resistors interrupt the center conductor of the CPW, and the JJ array forms a tee geometry with them, as shown schematically in Fig. 1(a) and a drawing is shown in Fig. 1(b). Input drive current pulses, with peak amplitude above the critical current ($I_c = 8$ mA) of the JJs, cause each junction to briefly switch to the voltage state (more accurately, the superconducting phase rotates by 2π) and releases a quantized voltage pulse before returning back to the superconducting state. The time-integrated area of each SFQ pulse is

$$\int V dt = \Phi_o \equiv h/2e \tag{1}$$

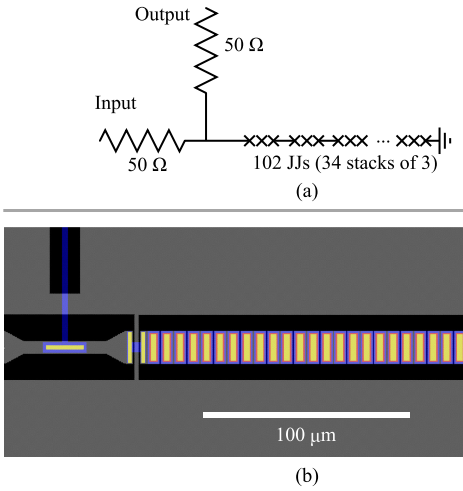

FIGURE 1. (a) Electrical schematic and (b) computer-aided design drawing of the JAWS circuit: grey indicates the base metal layer (niobium), red denotes self-shunted Nb/Nb-Si/Nb JJs in stacks of three, and yellow are vias between the base metal layer and blue wiring layer (niobium) or to make contact with the tops of the JJ stacks. Not shown in (b) are the 50 Ω on-chip resistors. The input dc bias and microwave pulses enter from the left side of the drawing and are shorted to ground on the far right side. If the input exceeds the critical current of the JJ array, a voltage is produced at the voltage tap (blue wire) and is sent to the quantum circuits.

where h is Plank's constant, e is the electron charge, and Φ_o is the magnetic flux quantum. To ensure that each junction in the array switches synchronously, we designed and fabricated self-shunted Nb/Nb-Si/Nb JJs (the JJ barrier material is niobium-doped silicon) with an I_cR product of $V_c = 43\,\mu$V, where R is the self-shunting resistance of 5.4 mΩ. This results in overdamped junction dynamics with characteristic time $\tau = \Phi_o/I_cR = 48$ ps; this time is much shorter than other relevant timescales of our experiment. Since the time duration of the SFQ pulse is set by $\sim 4\tau$, and area set by Φ_o (≈ 2.07 mV· ps), each pulse from the array has a maximum voltage of about 0.04 mV. When delivered to the 50 Ω load, the JAWS array produces approximately −68 dBm of microwave power when driven with the delta-sigma code described below [12].

We note that the JAWS circuit used in this article departs from typical designs used for voltage metrology in two important ways: our circuit has fewer junctions in the series array, and we use 50 Ω resistors to impedance match the transmission lines and measurement electronics [13]. Fewer junctions are required because only low power microwave signals of < −100 dBm are needed for qubit applications at ∼10 mK. Smaller arrays also have the benefit of reduced time-of-flight pulse broadening of the combined pulse signal [12], [14]. In the experiments described below, we used an array of 102 JJs consisting of 34 three-JJ stacks distributed evenly along an extent of about 200 μm to generate a −68 dBm JAWS signal. This signal was then attenuated by 30 dB to thermalize and attenuate the 4 K noise on the way to 10 mK to generate signal amplitudes appropriate for qubit control. The next section describes how qubit-relevant

IEEE Transactions on Quantum Engineering

signals are correctly synthesized at frequencies $f_{\rm syn} \simeq$ 4–8 GHz using this modified JAWS circuit design.

As described earlier, the JJs in the array need to be driven above I_c to produce SFQ pulses. For this experiment, a room-temperature pulse generator provides a delta-sigma encoded pulse stream with the pulse density modulated in time and with a maximum pulse density of $f_{\rm clock} \approx$ 14–16 gigapulses/s. This pulse density can be varied to produce different output powers and phases (if producing multiple tones), and the clock frequency can be varied to produce different output frequencies [12], [15]. The room temperature pulse generator produces pulses with rise/fall times of around 18 ps, and all connections to the input side of the JAWS array are high-bandwidth microwave components, i.e., 2.4 mm connectors rather than SMA, so as to minimize distortion of the input pulses at the JAWS chip. When measured at the intended synthesis frequency ($f_{\rm syn} \ll f_{\rm clock}$), this technique of microwave synthesis with JJs produces pure signals with large spurious-free dynamic range in a frequency bandwidth of $\ll f_{\rm syn}$ [16], [17]. An additional dc bias offset current is supplied through room temperature bias tees to ensure the JJs are operating in the quantum-locked range.

A (14–16) GHz pulse rate does not have a high enough oversampling ratio (we typically want $f_{\rm clock}/f_{\rm syn} \gg 10$) to synthesize frequencies above about 1 GHz with a good signal-to-noise ratio. To overcome this, we add extra zeros to the delta-sigma encoding. Here, a zero indicates no pulse and a one indicates a pulse. This *zero-padding* technique reduces the overall pulse density by a factor of three, and therefore reduces the synthesis frequency and generated amplitude proportionally, but creates aliased frequencies in upper Nyquist zones at frequencies of interest [18]. However, the key attributes of the JAWS output are preserved: the quantum locking range remains unchanged, the quantum-based output stability and accuracy are preserved, and, as described below, the noise shaping resulting from the delta-sigma encoding is also manifest in the upper Nyquist zones. A pedagogical example is shown in Fig. 2, showing the effect of zero-padding a 1 GHz tone and the aliasing to higher Nyquist zones [18].

A single one actually consists of two negative half-amplitude pulses around a central full-amplitude pulse such that the average level is zero over the full pulse sequence. Importantly, the negative pulses do not have enough amplitude to switch the junctions so do not contribute to the signal generated [16], [17]. In the end, this *zero-padded* and *zero-compensated* pulse sequence was designed to output 5.14 GHz (570-MHz tone aliased above a 4.57 GHz Nyquist frequency) when driven at an effective $f_{\rm clock} = 16$ GHz. Our room temperature electronics' clock, $f_{\rm clock}$, can then be changed to sweep $f_{\rm syn}$ over (5.14−4.33) GHz, which covers the frequency range needed to detect resonances in our qubit. The delta-sigma code used for the qubit measurements below is 131 072 b long after zero padding. The pulse sequence is generated at room temperature using a fourth-order delta-sigma algorithm in software. A similar technique was used for the resonator. Fig. 3(a) and (b) shows a sketch of these two

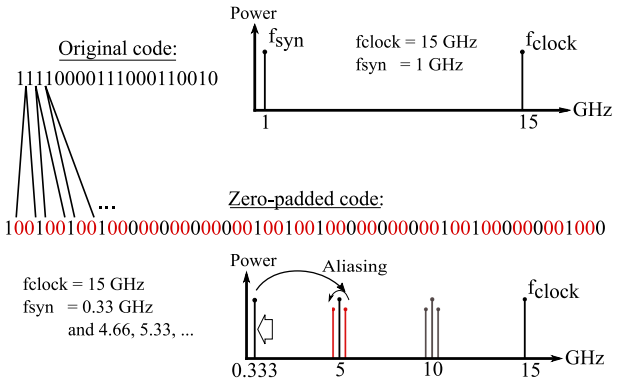

FIGURE 2. Example showing how a delta-sigma encoded waveform (the code sent to the JAWS from room temperature) is padded with zeros. This reduces the synthesized frequency by a factor of three, but aliases that signal to higher Nyquist zones around $f_{\rm clock}/3$ and $2f_{\rm clock}/3$. The sidebands around 5 GHz were used to drive the linear cavity and qubits in this article. Changing $f_{\rm clock}$ allows for those tones to be swept through the resonance of the device under test.

measurements. Our pulse density was chosen to produce an output power of −68 dBm.

To improve spectral purity in the waveform spectrum around the frequencies of interest, the delta-sigma algorithm's loop filter is a six-pole bandpass filter that reduces the digitization noise in a bandwidth of 60 MHz centered on the baseband frequency of interest. This region of improved spectral purity is also present in the higher Nyquist zones. Fig. 3(d) and (e) shows that the noise around the aliased central tone is, as expected, also reduced and pushed to higher and lower frequencies. The out-of-band noise was not filtered nor did it affect the linear resonator experiment shown in Fig. 3(a). However, later experiments with (nonlinear) qubits [see Fig. 3(b)] required careful filtering of this noise. The noise reduction around the synthesized tone is maintained *only* in the quantum locking range for the JAWS, where one input pulse corresponds to one and only one output pulse. This was confirmed by measuring the output spectrum while sweeping the dc bias current to the JAWS circuit across the full quantum locking range and to zero. This also serves to quantify the amount of feedthrough, i.e., room-temperature-generated input signal reaching the output [12]. When biased and filtered correctly, this ON/OFF ratio is greater than 60 dB. This ratio is adequate for quantum information applications.

III. RESONATOR MEASUREMENT

In the first experiment described here, we connect the JAWS output to a circuit consisting of a niobium CPW feedline with a $\lambda/4$ resonator capacitively coupled to it [see Fig. 4(a)]. The two chips were thermally anchored to copper packages with indium solder, bolted to the 4 K stage of a closed-cycle cryostat, and connected to one another via wirebonds and semirigid coaxial line. The resonator was designed to have a resonant frequency of 5.5 GHz. To perform spectroscopy of this circuit, we swept the synthesized frequency from 5.5 to 5.65 GHz. At each synthesized frequency, a spectrum

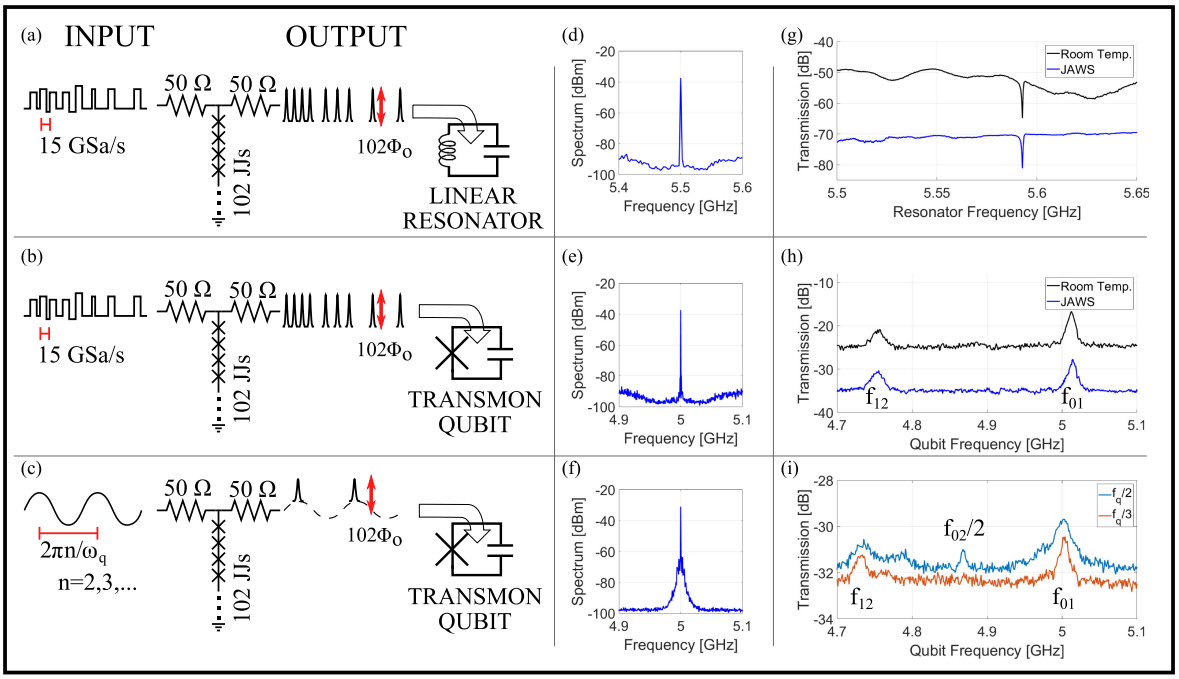

FIGURE 3. **Schematics of the first two experiments: the use of a room temperature pulse source to create SFQ pulses from a JAWS circuit to drive (a) a linear resonator and (b) a transmon qubit. (c) Alternative scheme, also demonstrated, where the JAWS array is excited with a CW drive and results in equally time-spaced SFQ pulses used to excite the same transmon. (d)–(f) Amplified spectra taken near the resonator and qubit frequency of all three techniques. (g) Compares the resulting spectroscopy between a room temperature (black, offset) and JAWS (blue) excitation of the linear resonator. (h) Compares spectroscopy of the transmon driven with a room temperature microwave source (black, offset) and with JAWS (blue). (i) Qubit spectroscopy using a CW drive to the JAWS at ω_q/n, where $n = 2$ (blue) and $n = 3$ (orange) resulting in different power being delivered to the qubit. Note that the difference in qubit frequency in (h) and (i) is due to the fact that they were taken during different cooldown cycles of the ADR.**

analyzer was used to measure the microwave power that was transmitted through the resonator chip to room temperature. The results of this measurement are plotted in Fig. 3(g) in blue. There was approximately 2 dB of loss (from cabling, connectors, etc.) between the resonator and spectrum analyzer; thus, the off-resonant transmission of about −70 dBm is consistent with our estimates above. To confirm our JAWS measurement, we also set up a 10 dB directional coupler so that we could use a room-temperature microwave source to perform the same experiment, i.e., comparing results between ports one and three versus ports two and three in Fig. 4(a). The black trace (offset by +30 dB) in Fig. 3(g) shows those room temperature microwave source data. The off-resonant data show more ripple from the room temperature source, most likely from additional connectors, cabling, and slight impedance mismatches. Generation of the probe signal at 4 K avoids those effects. Our delta-sigma encoding allows waveform synthesis with precise programming of the phases of single and multiple, closely spaced tones [12]. These attributes make possible traditional homodyne or heterodyne measurements, as well as more complex microwave network analysis.

IV. QUBIT MEASUREMENT I

To demonstrate the JAWS's applicability for quantum computing applications, we next moved the JAWS package to the 4 K stage of an adiabatic demagnetization refrigerator (ADR) and connected the output to a typical qubit measurement chain (attenuation, magnetic shielding, and filtering), as shown in Fig. 4(b). By mounting the qubit at 100 mK, higher level energy states of the qubit are thermally occupied and, thus, can be excited easily with our JAWS circuit and do not require two tones as needed at lower temperatures. Unfortunately, measurements of coherence (e.g., T1, T2) are not possible at these higher temperatures and limited hold times but will be performed when the experiment is moved to a dilution refrigerator.

The transmon qubit used for this experiment is capacitively coupled to a $\lambda/2$ CPW readout resonator (fundamental frequency $\omega_r/2\pi = 7.016$ GHz) with a coupling strength $g/2\pi = 59$ MHz. The capacitor of the transmon qubit is comprised of a circular pad and concentric ring with a gap to avoid flux trapping. The qubit capacitor is shunted with two nominally identical Al/AlO $_x$/Al JJs each with $I_c = 30$ nA in a SQUID geometry. The JJs are fabricated using an overlap technique [19]. The area of the SQUID loop is about 200 μm^2 and an on-chip flux bias line is used to tune the qubit frequency. In this experiment, the transmon qubit is tuned to $\omega_q/2\pi = 5$ GHz with the anharmonicity $\alpha/2\pi = 250$ MHz ($\alpha = |\omega_{12} - \omega_{01}|$, where ω_{nm} refers to the nth and mth energy levels of the qubit). The circuit, except for the JJs, is made of thin film NbTiN.

By including directional couplers in our measurement setup [see Fig. 4(b)], we are able to separately perform qubit

IEEE Transactions on Quantum Engineering

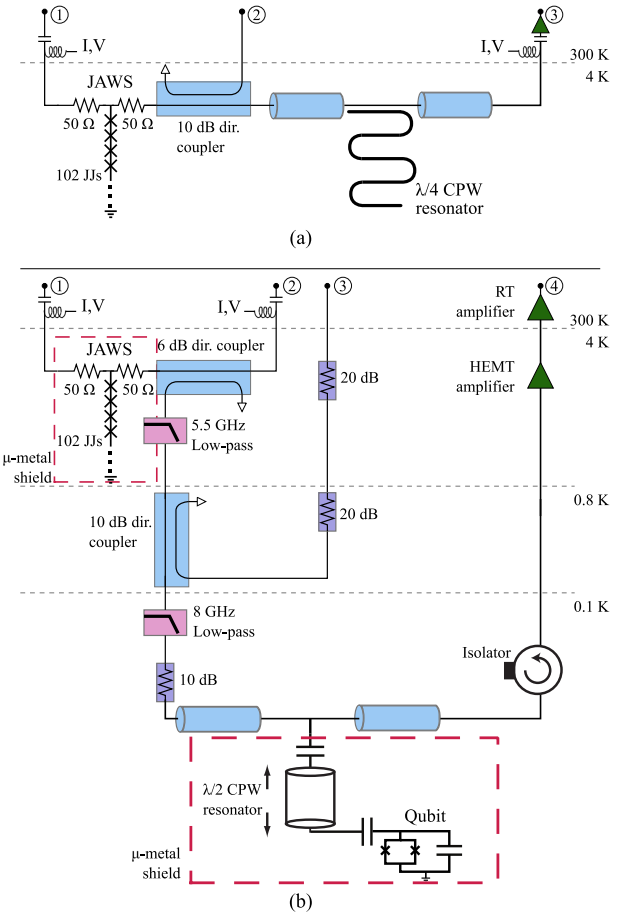

FIGURE 4. Measurement schematics for two experiments. (a) JAWS driving a linear resonator. (b) JAWS driving a qubit coupled to a resonator. In each case, directional couplers are used to enable comparison between signals generated at room temperature versus signals generated at 4 K.

spectroscopy with room temperature microwave sources (through ports three and four) or with the JAWS source (through ports one and four). By connecting a spectrum analyzer to the output of the amplifier chain (high-electron-mobility transistor (HEMT) and room temperature amplifiers with a total gain of about 70 dB), we first compared both the JAWS and room temperature sources at slightly different frequencies and confirmed that the amplitudes of both signal sources were equal over the full range of interest. This accounts for unknown insertion losses in the measurement chain and confirms again that the JAWS remains in its quantum locked mode throughout the full spectroscopy range. The microwave power delivered to the qubit is about −100 dBm in both cases after accounting for insertion losses and attenuation.

We then performed CW qubit spectroscopy with each of the microwave sources individually. We swept the JAWS frequency (port 1) while monitoring the resonator's response in transmission with a vector network analyzer through ports 3 and 4 [20]. Port 2 acts as a return path for the dc bias, and as a way to monitor the delta-sigma input, if needed. The results of these measurements are plotted in Fig. 3(h)—the blue trace while being driven by the JAWS, and black trace being driven by the room temperature microwave source (black, offset by +10 dB for clarity). Both closely agree with one another and show the ω_{01} and ω_{12} qubit transition frequencies. The difference in these frequencies also matches the qubit's designed anharmonicity of 250 MHz. We note that in order to avoid directly stimulating the higher qubit transitions, our delta-sigma code was also carefully designed and checked to not have spurious signals at frequencies those unwanted transition frequencies and only one transition was being excited at any one time.

As discussed earlier, using delta-sigma encoded signals to produce spectroscopy tones also produces signals in the third Nyquist zone around 7.2 GHz in our case. For example, filtering was needed to attenuate the signals at those frequencies to minimize their interaction with the resonator (and harmonics of the resonator), qubit, or HEMT. These filters could easily be co-fabricated on chip to mitigate these spurious tones in future designs. This change could also produce pure, accurate, and reproducible tones that may be useful as a stable local oscillator signal for heterodyne readout, for example.

V. QUBIT MEASUREMENT II

An alternative qubit drive method can, instead, produce *pulse trains* at 4 K with enough amplitude to perform qubit spectroscopy with the same array [5]. If one drives the JAWS circuit with a CW microwave signal, Shapiro steps (the CW analog of the quantum locking range) are obtained [21]. The width of these steps indicate the range over which the bias current can be swept where one, and only one, quantized voltage pulse per junction is generated per CW period [see Fig. 3(c)]. Similar to work presented in [5], to avoid directly driving the qubit with the input CW tone, we drive with an integer fraction of the qubit frequency, in this case, $\omega_q/2$ or $\omega_q/3$. The SFQ pulses generated in this manner have spectral content at the qubit frequency and can again be swept to perform qubit spectroscopy.

In Fig. 3(i), we show the response of the qubit by sweeping the JAWS through $\omega_q/2$ (blue) and $\omega_q/3$ (orange). The $\omega_q/2$ sweep ($2\pi \times$(2.55–2.35) GHz) shows the $\omega_{02}/2$ transition as well as the ω_{01} and ω_{12}, whereas the $\omega_q/3$ signal ($2\pi \times$(1.70–1.57) GHz) shows only the ω_{01} and ω_{12} transitions, as expected from a lower average power drive. The difference in power delivered to the qubit is due to the difference in time density of pulses, i.e., the period between pulses is longer for lower frequency signals.

Fig. 3(f) shows the resulting spectrum of the JAWS output. When compared to the (sharp) input pulse driven technique of Fig. 3(e), this CW input drive technique has much slower rise time that results in increased random timing jitter/phase noise in the generated pulses. In other words, this noise is a result of the characteristic time of the JAWS JJs being much smaller than the CW period, $\tau \ll 1/2.5$ GHz. The junctions respond quickly to the drive tone and, therefore, any dc current noise in the drive is efficiently converted to phase noise

of the JAWS output. A simple design change, reducing I_cR by fabricating a new JAWS device, will significantly reduce the phase noise. Different amplitude signals would also be possible by fabricating arrays with more or fewer JJs.

VI. CONCLUSION

As 4 K signal generation and processing matures, we expect that the generation of quantized pulse sequences *without* room temperature electronics will be realized. In this article, we used a simple JJ array to demonstrate two techniques for generating qubit control signals. High-speed SFQ electronics also show promise to synthesize more complex waveforms. To that end, we have demonstrated an SFQ-based voltage multiplier circuit that can produce 40 GHz SFQ pulse streams when driven by a room temperature source [15], [22] without needing to use the second Nyquist zone. With room temperature electronics providing the input pulse streams, this circuit was used to digitally synthesize a shaped microwave pulse with a 4 GHz tone and 200 ns Gaussian amplitude envelope. To produce such pulse-shaped microwave signals required a significant depth of room-temperature memory to store the complex delta-sigma code, which currently limits the feasibility of deploying at 4 K a combined SFQ synthesizer chip with sufficient memory. However, adding an SFQ-based circular shift register with a depth of $\simeq$100 b to store simpler pulse trains or separately integrating SFQ circuits with cryogenic-capable CMOS memories are areas of active research [5], [10], [23], [24].

Locating control and readout electronics inside the cryostat at 4 K and closer to the qubits is a first step toward building a more compact, scalable cryogenic quantum computer. This path offers reduced latency and dramatically reduced heat load from the number of microwave cables required from room temperature. Dissipation at the 4 K stage can be further reduced by driving the JAWS control circuits via an optical link [25] and using energy-efficient superconducting SFQ electronics [26] and interconnects. Superconducting cable counts and heat loads from 4 K to millikelvin may be improved by channelizing 4 K waveforms into a broadband coaxial line, then dechannelizing again at a lower temperature stage. These techniques are commonly used in RF communications at room temperature. SFQ-based electronics, with their high clock speeds, are ideally suited for such signal processing and for low-latency error detection and feedback schemes.

In conclusion, we have demonstrated that a 4 K JAWS circuit with minor modifications from designs that have proven metrological accuracy can be used to control devices useful for quantum information systems. These circuits can be used to drive resonators and qubits, and perform as stable, reproducible local oscillators. We compared the 4 K signal generation with room temperature signal generation, seeing no deleterious effects and indications that fewer impedance mismatches are in fact beneficial. In the near future, we plan to continue these experiments in a dilution refrigerator to demonstrate coherent pulse control and state initialization of transmon qubits using JAWS. We plan to use a JAWS circuit with ten times the number of JJs to produce 20 dBm higher output power to overcome the additional attenuation required for thermalization of the signal at the base temperature stage. With this setup, we will confirm that quasi-particle poisoning of the qubit is minimized by moving the SFQ electronics for qubit control from the qubit chip to the 4 K stage. Additionally, measurements of qubit coherence and gate fidelities will be performed to prove that programmable Josephson microwave sources are a viable path forward for scaling quantum computing systems.

ACKNOWLEDGMENT

The authors would like to thank D. Pappas and J. Long for use of their ADR and initial design, characterization, and testing of the qubit. The data that support the findings of this study are available from the corresponding author upon reasonable request.

REFERENCES

[1] M. H. Devoret and R. J. Schoelkopf, "Superconducting circuits for quantum information: An outlook," *Science*, vol. 339, no. 6124, pp. 1169–1174, 2013, doi: 10.1126/science.1231930.

[2] P. Krantz, M. Kjaergaard, F. Yan, T. P. Orlando, S. Gustavsson, and W. D. Oliver, "A quantum engineer's guide to superconducting qubits," *Appl. Phys. Rev.*, vol. 6, no. 2, 2019, Art. no. 021318, doi: 10.1063/1.5089550.

[3] F. Arute *et al.*, "Quantum supremacy using a programmable superconducting processor," *Nature*, vol. 574, pp. 505–510, 2019, doi: 10.1038/s41586-019-1666-5.

[4] N. E. Flowers-Jacobs, S. B. Waltman, A. E. Fox, P. D. Dresselhaus, and S. P. Benz, "Josephson arbitrary waveform synthesizer with two layers of Wilkinson dividers and an FIR filter," *IEEE Trans. Appl. Supercond.*, vol. 26, no. 6, Sep. 2016, Art. no. 1400307, doi: 10.1109/TASC.2016.2582800.

[5] R. McDermott *et al.*, "Quantum–classical interface based on single flux quantum digital logic," *Quantum Sci. Technol.*, vol. 3, no. 2, Jan. 2018, Art. no. 024004, doi: 10.1088/2058-9565/aaa3a0.

[6] E. Leonard *et al.*, "Digital coherent control of a superconducting qubit," *Phys. Rev. Appl.*, vol. 11, Jan. 2019, Art. no. 014009, doi: 10.1103/PhysRevApplied.11.014009.

[7] M. Beck, "Hybrid superconducting quantum computing architecture," Ph.D. dissertation, Dept. Physics, Univ. Wisconsin–Madison, Madison, WI, USA, 2018.

[8] G. Catelani, R. J. Schoelkopf, M. H. Devoret, and L. I. Glazman, "Relaxation and frequency shifts induced by quasiparticles in superconducting qubits," *Phys. Rev. B*, vol. 84, Aug. 2011, Art. no. 064517, doi: 10.1103/PhysRevB.84.064517.

[9] E. M. Leonard Jr., "Digital control of superconducting quantum bits," Ph.D. dissertation, Dept. Physics, Univ. Wisconsin–Madison, Madison, WI, USA, 2018.

[10] J. C. Bardin *et al.*, "Design and characterization of a 28-nm bulk-CMOS cryogenic quantum controller dissipating less than 2 mW at 3 K," *IEEE J. Solid-State Circuits*, vol. 54, no. 11, pp. 3043–3060, Nov. 2019, doi: 10.1109/JSSC.2019.2937234.

[11] S. Narayana, Y. A. Polyakov, and V. K. Semenov, "Evaluation of flux trapping in superconducting circuits," *IEEE Trans. Appl. Supercond.*, vol. 19, no. 3, pp. 640–643, Jun. 2009, doi: 10.1109/TASC.2009.2018248.

[12] C. A. Donnelly *et al.*, "1 GHz waveform synthesis with Josephson junction arrays," *IEEE Trans. Appl. Supercond.*, vol. 30, no. 3, Apr. 2020, Art. no. 1400111, doi: 10.1109/TASC.2019.2932342.

[13] A. Rüfenacht, N. E Flowers-Jacobs, and S. P Benz, "Impact of the latest generation of Josephson voltage standards in ac and dc electric metrology," *Metrologia*, vol. 55, no. 5, pp. S152–S173, Aug. 2018, doi: 10.1088/1681-7575/aad41a.

[14] C. A. Donnelly *et al.*, "Quantized pulse propagation in Josephson junction arrays," *IEEE Trans. Appl. Supercond.*, vol. 30, no. 3, Apr. 2020, Art. no. 1400208, doi: 10.1109/TASC.2019.2929481.

[15] M. A. Castellanos-Beltran, D. Olaya, A. J. Sirois, P. D. Dresselhaus, P. F. Hopkins, and S. P. Benz, "SFQ multiplier circuits for synthesizing gigahertz waveforms with quantum-based accuracy," *IEEE Trans. Appl. Supercond.*, submitted for publication.

[16] J. A. Brevik *et al.*, "Radio-frequency waveform synthesis with the Josephson arbitrary waveform synthesizer" in *Proc. Conf. Precis. Electromagn. Meas.*, Jul. 2018, pp. 1–2, doi: 10.1109/CPEM.2018.8501023.

[17] J. A. Brevik, N. E. Flowers-Jacobs, A. E. Fox, E. B. Golden, P. D. Dresselhaus, and S. P. Benz, "Josephson arbitrary waveform synthesis with multilevel pulse biasing," *IEEE Trans. Appl. Supercond.*, vol. 27, no. 3, Apr. 2017, Art. no. 1301707, doi: 10.1109/TASC.2017.2662708.

[18] Analog Devices, "A technical tutorial on digital signal synthesis," Analog Devices, Norwood, MA, USA, Tech. Rep., 1999.

[19] X. Wu, J. L. Long, H. S. Ku, R. E. Lake, M. Bal, and D. P. Pappas, "Overlap junctions for high coherence superconducting qubits," *Appl. Phys. Lett.*, vol. 111, no. 3, 2017, Art. no. 032602, doi: 10.1063/1.4993937.

[20] J. A. Schreier *et al.*, "Suppressing charge noise decoherence in superconducting charge qubits," *Phys. Rev. B*, vol. 77, May 2008, Art. no. 180502, doi: 10.1103/PhysRevB.77.180502.

[21] S. Shapiro, "Josephson currents in superconducting tunneling: The effect of microwaves and other observations," *Phys. Rev. Lett.*, vol. 11, pp. 80–82, Jul. 1963, doi: 10.1103/PhysRevLett.11.80.

[22] P. F. Hopkins *et al.*, "RF waveform synthesizers with quantum-based voltage accuracy for communications metrology," *IEEE Trans. Appl. Supercond.*, vol. 29, no. 5, Aug. 2019, Art. no. 1301105, doi: 10.1109/TASC.2019.2898407.

[23] F. Motzoi, J. M. Gambetta, S. T. Merkel, and F. K. Wilhelm, "Optimal control methods for rapidly time-varying Hamiltonians," *Phys. Rev. A*, vol. 84, Aug. 2011, Art. no. 022307, doi: 10.1103/PhysRevA.84.022307.

[24] Y. Hironaka, Y. Yamanashi, and N. Yoshikawa, "Demonstration of a single-flux-quantum microprocessor operating with Josephson-CMOS hybrid memory," *IEEE Trans. Appl. Supercond.*, vol. 30, no. 7, Oct. 2020, Art. no. 1301206, doi: 10.1109/TASC.2020.2994208.

[25] F. Lecocq, F. Quinlan, K. Cicak, J. Aumentado, S. A. Diddams, and J. D. Teufel, "Control and readout of a superconducting qubit using a photonic link," in *Proc. OSA Quantum 2.0 Conf.*, 2020, Art. no. QM6A.3, doi: 10.1364/QUANTUM.2020.QM6A.3.

[26] O. A. Mukhanov, "Energy-efficient single flux quantum technology," *IEEE Trans. Appl. Supercond.*, vol. 21, no. 3, pp. 760–769, Jun. 2011, doi: 10.1109/TASC.2010.2096792.